Turkish Journal of Electrical Engineering & Computer Sciences

http://journals.tubitak.gov.tr/elektrik/

Research Article

Turk J Elec Eng & Comp Sci
(2020) 28: 2483 – 2492

doi:10.3906/elk-1909-44

Wavelength sensitivity of indium tin oxide on surface plasmon resonance angles

Antonio A. RUIZ-RAMIREZ*, **Carlos VILLA-ANGULO**, **Ivan O. HERNANDEZ-FUENTES**
Institute of Engineeering, Autonomous University of Baja California, Mexicali, Mexico

Received: 07.09.2019 • **Accepted/Published Online:** 08.01.2020 • **Final Version:** 25.09.2020

Abstract: Surface plasmon resonance (SPR) is a charge-density oscillation that occurs when a beam of p-polarized monochromatic light impinges with a greater angle than the critical angle in a dielectric-metal interface. Because of the high losses related to metals, the generated surface plasmon waves propagate with high attenuation in the visible and near-infrared spectral regions in most of the dielectric-metal interfaces. An alternative to reduce such losses is to use a transparent indium tin oxide (ITO) film. In this paper, we compared theoretical calculations and experimental measurements of the SPR angle θ_{SPR} on the interfaces of a borosilicate prism (Bp) and ITO, Bp-Ag, and Bp-Au. Three different wavelengths (405, 532, and 650 nm) were used to measure θ_{SPR} that covered almost all of the visual range spectrum. Both calculations and experimental data showed that SPR characteristics are strongly influenced by the metal's optical properties. The measured θ_{SPR} in the Bp-ITO interface is much smaller than the θ_{SPR} measured in the other two interfaces. Hence, ITO can be used in a similar way as Au and Ag in prism-metal interfaces, providing a cheaper and more versatile option to generate the SPR effect.

Key words: Surface plasmon resonance, borosilicate prism, indium tin oxide, silver, gold

1. Introduction

Over the last three decades, scientific communities in the areas of gas detection, characterization of thin films, monitoring processes at metal interfaces, and biosensing have increased their attention in the development of surface plasmon resonance (SPR) [1–5], due to the possibility that SPR offers real-time measurement of physical, chemical, and biological quantities [6]. Characteristics such as field observations and analysis of biomolecular interaction without the use of labeled molecules provide certain advantages to SPR compared with a variety of optical methods used for chemical and biochemical sensing and characterization. These methods include ellipsometry, interferometry, and spectroscopy of guided modes in optical waveguide structures [7–10].

SPR is a charge-density oscillation that may exist if a beam of p-polarized monochromatic light impinges with a greater angle than the critical angle in a dielectric-metal interface. The generated charge density wave is associated with an electromagnetic wave. The field vector of this electromagnetic wave reaches its maximum at the interface and decays exponentially into both media. This wave is known as a surface plasma wave (SPW) and it is also a TM-polarized wave [11]. Most of the electromagnetic field of a SPW is concentrated in the dielectric material and is distributed in a highly asymmetrical fashion along the two interface materials. The SPW propagation may be supported by structures where the dielectric constant of the metal, ϵ_m, is less than the square of the negative refractive index of the dielectric, ϵ_d^2 [12]. This condition is fulfilled by several

*Correspondence: antonio.adolfo.ruiz.ramirez@uabc.edu.mx

dielectric-metal interfaces where the most commonly used metals are gold (Au) and silver (Ag) [13]. It has been reported several times that SPW propagating along the surface of a dielectric-Ag interface is less attenuated and exhibits higher localization of the electromagnetic field in a dielectric than SPW propagating in a dielectric-Au interface [14, 15]. High loss occurs in metals resulting in the propagation of a SPW with high attenuation in the visible and near-infrared spectral regions in most of the studied dielectric–metal interfaces [16, 17].

Due to the current demand for massive production of SPR effect devices as well as economic illumination sources in the visible and near-infrared spectral ranges, alternative materials that support the generation of SPWs are required [18–20]. An alternative for metals is the use of transparent conductive oxide (TCO) thin films. These types of materials are used in different technologies such as biosensors, flat panels, and photovoltaics because of their good electrical conductivity and optical transparency properties [21]. TCOs have good electrical conductivity and low absorbability of light; they are often fabricated with thin-film technologies and utilized in optoelectronic applications, such as transparent electrodes in touch panels and flat-panel displays. Besides these applications, TCO thin films are used as electrode materials in biosensor and sensor technologies [22]. The most commonly used TCO is tin-doped indium oxide, In2O3:Sn1 (In2O3eSnO2), known as indium tin oxide (ITO) [23]. ITO is not a transition metal but it is an oxide made of two posttransition metals. Therefore, its optical characteristics are slightly different from those of a transition metal. Its low absorbability can be used to improve SPR generation and detection.

In this paper we compared theoretical calculations and experimental measurements of θ_{SPR} on an interface made of Bp-ITO, Bp-Ag, and Bp-Au. Three different wavelengths (405, 532, and 650 nm) were used to measure the SPR angle through the edges and middle wavelength of the visual range spectrum. Both calculations and experimental data showed that SPR characteristics for the three studied interfaces were strongly influenced by the metal properties. Moreover, quite different regularities of plasmon excitation and sensing response were observed for the three different wavelengths in each interface. Specifically, the measured θ_{SPR} in the ITO interface showed much smaller values than θ_{SPR} measured in the interfaces with Ag and Au. This can be attributed to ITO's low absorption of light in the visual range spectrum, which makes ITO useful when monochromatic light from a laser source is replaced by a white light source with an interferential filter and a polarizer.

2. Theoretical formulation

SPR is generated under two general conditions: a beam of p-polarized monochromatic light hitting a dielectric-metal interface, and the total internal reflection (TIR) taking place in such an interface. TIR occurs if the refractive index of the dielectric (n_1) is higher than the refractive index of the metal (n_2) and also if the angle of the incident beam, θ, is greater than the critical angle, given by $\theta c = sin^{-1}(n_2/n_1)$. Hence, the electromagnetic evanescent waves are guided along the boundary (interface) of two media, as shown in Figure 1. The field of these evanescent waves penetrates into the adjacent media, decaying exponentially until it vanishes at a given distance from the interface. The magnitude of the parallel wave vector of the evanescent wave, $k_{x,||}$, is expressed in Equation (1) [24] as follows:

$$k_{x,||} = n\frac{\omega}{c}sin(\theta), \tag{1}$$

where n is the refractive index of the evanescent wave traveling media, c is the speed of light, $\omega = 2\pi/\lambda$, ω is the angular frequency, and λ is the wavelength of the incident light.

Additionally, the dielectric constants of both the dielectric and the metal film are related to the magnitude of the wave vector, k_{SP}, of the evanescent waves, which penetrates into the adjacent media of the interface according to Equation (2) [11, 25]. This is applicable in nonabsorbing media where the dielectric constant equals the square of the refractive index:

$$k_{SP} = \frac{2n}{\lambda c}\sqrt{\frac{n_3^2 n_2^2}{n_3^2 + n_2^2}}, \tag{2}$$

where the refractive index of the dielectric, metal, and air are represented as n_1, n_2, and n_3, respectively.

The SPR is generated by the excitation of the surface plasmon from the evanescent waves at the dielectric-metal interface. Once TIR is reached by tuning the angle of the monochromatic incident beam, θ, the intensity of the reflected waves decreases sharply, and evanescent waves penetrate into the adjacent media, decaying exponentially until they reach a given distance from the interface. Hence, SPR requires that k_{SP} equals $k_{evan,||}$ [26]. Furthermore, the SPR angle, θ_{SPR}, is obtained using Equation (1) and Equation (2) to give Equation (3):

$$\theta_{SPR} = sin^{-1}\left(\frac{1}{n_1}\sqrt{\frac{n_3^2 n_2^2}{n_3^2 + n_2^2}}\right). \tag{3}$$

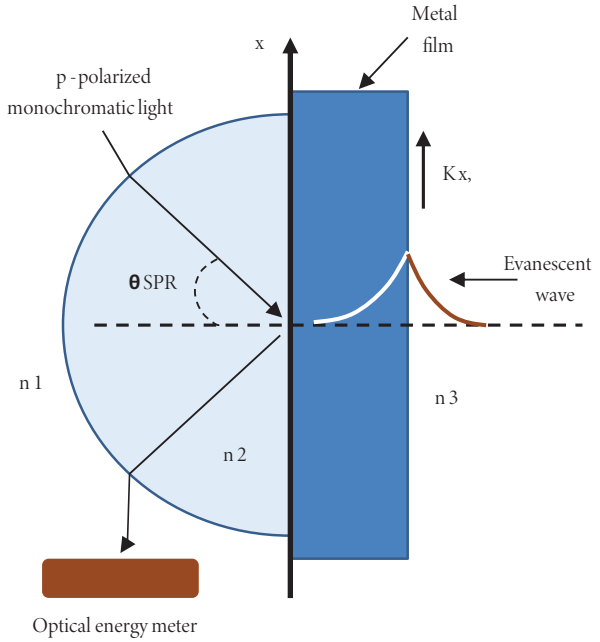

Figure 1. Schematic diagram of the prism-metal-air system used to generate the SPR.

3. Practical implementations

The experimental setup constructed to demonstrate excitation and measurement of SPR at multiple wavelengths and multiple angles is shown in Figure 2. SPR occurs on the interface of three sets of dielectric-metal interfaces: a Bp prism and a 200-nm Ag layer, a Bp prism and a 200-nm Au layer, and a Bp prism and an ITO layer. As shown in Figure 2a, monochromatic light from a 5-W class IIB laser is focused towards a polarizer lens

that p-polarizes it. Furthermore, the p-polarized light impinges the Bp prism, creating the prism's incident angle, θ_1. Likewise, the prism's inner angle θ_2 (obtained by Snell's law) deflects the light and makes it hit the prism-metal interface. A small amount of light is deflected and the rest is reflected out of the prism. Finally, the reflected light is sensed by an optical power meter. Figure 2b shows a picture of the alignment of the physical component of the SPR setup system. The separation distance between the laser source and the p-polarized lens is 30 cm, while 20 cm is the distance between the p-polarizer and the prism-metal interface. Figure 2c shows a picture of the SPR effect given at the reflected plane of the prism-metal interface. The prism-metal interface is mounted on a circular rotator that is turned to obtain the SPR effect in the reflected plane.

4. Calculations and measurement results

The calculations and experimental data revealed that the SPR effect was produced by the three interfaces (Bp-ITO, Bp-Ag, and Bp-Au) studied under three different wavelengths (405, 532, and 650 nm) used to illuminate the interfaces. Additionally, the SPR angle, θ_{SPR}, was theoretically calculated using Equation (3) and the complex refractive index, ñ, as shown in Table 1. The complex refractive index for air was considered to be 1. Figure 3 shows, for 405-nm illumination wavelength, the measured angular reflectivity curves for Ag (dashed curve), Au (dotted curve), and ITO (solid curve). Also, θ_{SPR} obtained from practical measurements and θ_{SPR} obtained from theoretical calculations are shown in Table 2. From Figure 3 it is observed that the SPR effect was achieved at quite different θ_{SPR} angles for each of the three prism–metal interfaces. This behavior can be attributed to the practical low sensitivity of the Bp-metal interface to optical excitation wavelengths approaching the ultraviolet spectrum. Therefore, the main trend of theoretical prediction was confirmed by relevant experimental data and theoretical calculations. As expected, the calculated and measured positions of minimum reflectivity were almost identical for the three prism-metal interfaces, which confirms the validity of the applied plasmon model used in the calculations and the relative precision of the data obtained from measurements. Table 1 shows the experimental values for the refractive indices of Ag, Au, and ITO at 405 nm, 532 nm, and 650 nm for each material [27–30].

Table 1. Complex index of refraction.

Wavelength (λ)	Complex index of refraction (ñ)			
	Ag	Au	ITO	Prism
405 nm	$0.052478 + 2.1966i$	$0.46447 + 4.7022i$	$2.1066 + 0.042872i$	$1.5334 + 6.5853^{-7}i$
532 nm	$0.051781 + 3.4215i$	$1.51280 + 2.3083i$	$1.9327 + 0.046741i$	$1.5225 + 5.4382^{-8}i$
650 nm	$0.049517 + 4.414i$	$1.35050 + 2.0324i$	$1.8478 + 0.046741i$	$1.5174 + 2.6^{-8}i$

Table 2. θ_{SPR}, measurements, and theoretical calculations.

Metal	Ag			Au			ITO		
Wavelength (λ)	405 nm	532 nm	650 nm	405 nm	532 nm	650 nm	405 nm	532 nm	650 nm
θ_{SPR} calculated	33.8125°	30.2326°	29.2362°	32.1219°	31.1838°	30.3981°	21.7848°	20.2532°	19.3796°
θ_{SPR} measured	32.9504°	31.0154°	30.1256°	29.9289°	28.5672°	28.5647°	21.2290°	19.4569°	18.3332°

Figures 4 and 5 show, for 532-nm and 650-nm illumination wavelengths, respectively, the measured angular reflectivity curves for Ag (dashed curve), Au (dotted curve), and ITO (solid curve). The calculated and

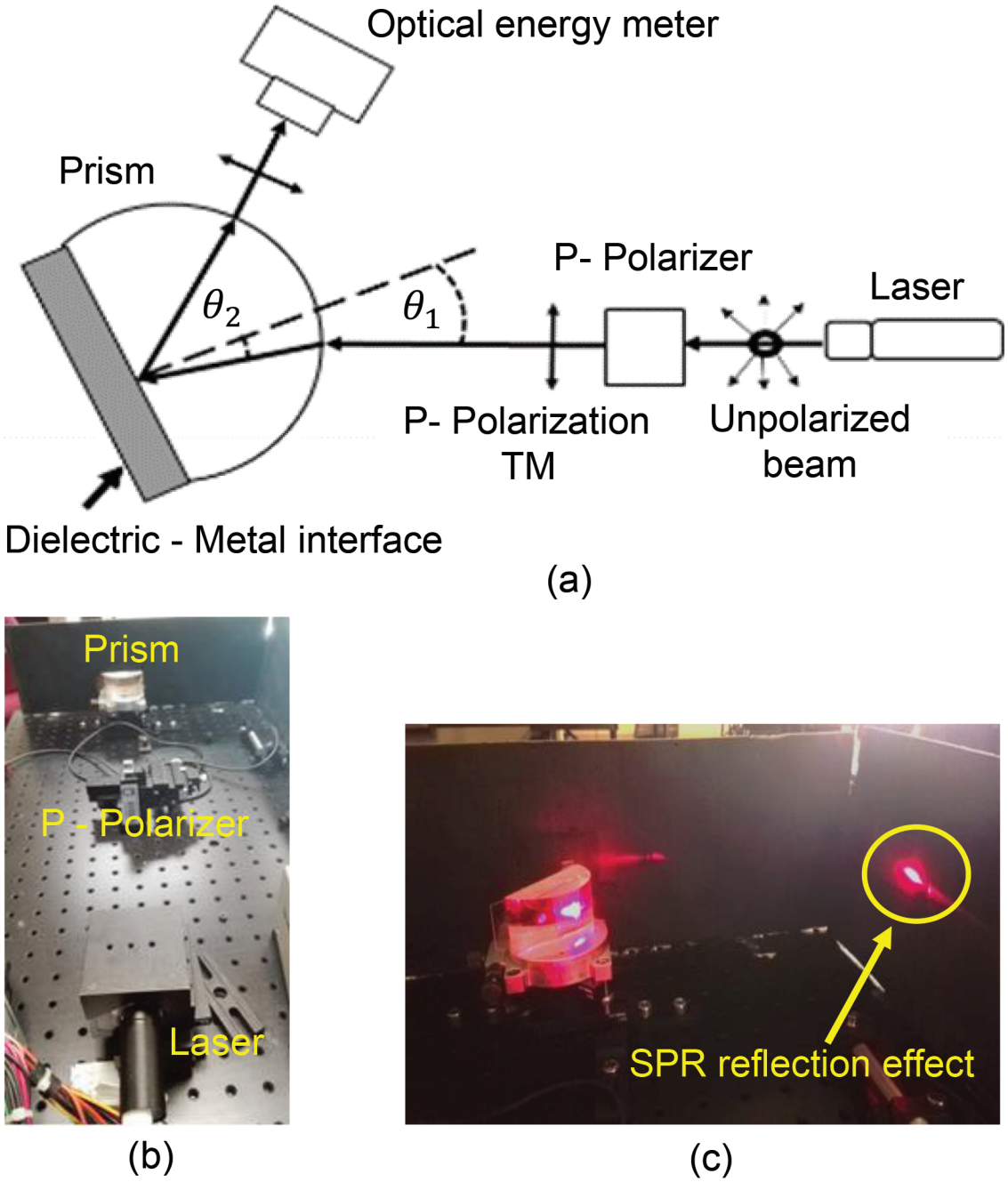

Figure 2. Experimental setup of the system used to obtain the SPR. (a) Schematic diagram of the SPR setup experiment. (b) Picture of the alignment of physical component of the SPR setup. (c) Picture of the SPR effect given at the reflected plane of the prism-metal interface.

measured θ_{SPR} are also shown in Table 2. Similar to the 405-nm wavelength, the main trends of theoretical predictions for 532 nm and 650 nm were confirmed by experimental measurements. From plots depicted in Figures 4 and 5 and calculations shown in Table 2, it is observed that θ_{SPR} decreases with the increase in the wavelength of incident light. This decrease in θ_{SPR}'s behavior is similar to the behavior of the real part of the

refractive index, which also decreases. For example, considering the wavelengths from 405 to 650 nm, θ_{SPR} angles decrease from 32.9504° to 30.1256° in the case of Ag, while the real part of the refractive index decreases from 0.052478 to 0.049517. For Au, θ_{SPR} angles decrease from 29.9289° to 28.5647° while the real part of the refractive index decreases from 1.5652 to 0.11114. Finally, for ITO, θ_{SPR} angles decrease from 21.2290° to 18.3332° while the real part of the refractive index decreases from 2.1066 to 1.8478. Because the refractive index describes how fast light propagates through the material, the θ_{SPR} angle is directly proportional to the speed of light propagating on the prism-metal interfaces. Also, from Figures 3–5, it is observed that the dispersion width of the minimum reflectivity increases as the wavelength increases and decreases as the index of refraction increases. For example, the full width at half maximum (FWHM) at 405 nm for Ag, Au, and ITO is 2.51°, 2.60°, and 2.62°, respectively; the FWHM at 532 nm for Ag, Au, and ITO are 2.40°, 2.85°, and 2.91°; and the FWHM at 650 nm for Ag, Au, and ITO are 3.9°, 4.43°, and 4.98°, respectively. The smallest FWHM is obtained for Ag at 405 nm, while the largest is for ITO at 650 nm. The smallest value is apparently attributed to the relatively low real part of the refractive index of Ag, while the largest is attributed to the relatively high real part of the refractive index of ITO.

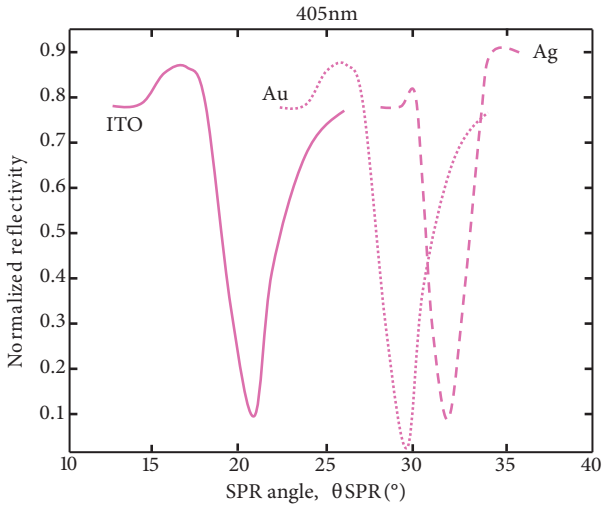

Figure 3. At 405-nm illumination wavelength, measured angular reflectivity curves at Ag (dashed curves), Au (dotted curve), and ITO (solid curve).

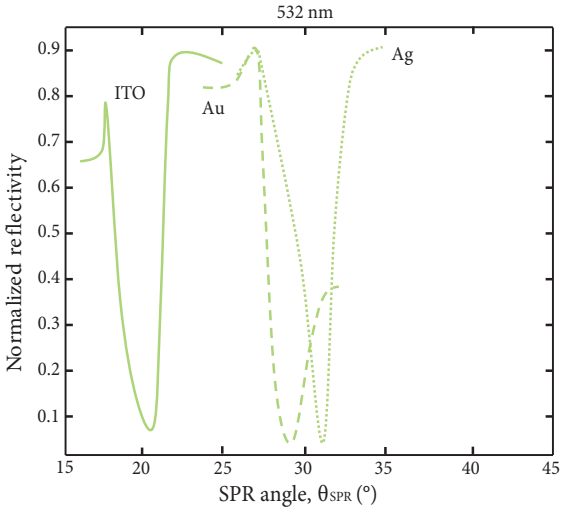

Figure 4. At 532-nm illumination wavelength, measured angular reflectivity curves at Ag (dashed curves), Au (dotted curve), and ITO (solid curve).

The data for the SPR minimum position collected from the angular and spectral reflectivity curves are summarized in Figure 6, which describes the resonant conditions for simultaneous variation in λ and θ. As illustrated in this figure, the three SPR dispersion curves show similar behavior, which means that the SPR angle decreases with increases in wavelength. It is important to note that, in the Bp-ITO interface, the measured θ_{SPR} ranges from 21.2290° to 18.3332°, which is much smaller than θ_{SPR} measured in the other two interfaces. There are more than eight degrees and more than seven degrees of difference comparing the Bp-ITO interface with the Bp-Au and Bp-Ag interfaces, respectively. The smaller θ_{SPR} for the Bp-ITO interface could be explained by considering conditions of wavenumber matching in terms of the dispersion $\omega(k_x)$ as described in Figure 7.

Qualitative behavior of the dispersion relations of the surface plasmon wave at the Bp-Ag, Bp-Au, and Bp-ITO interfaces are shown in Figure 7. To interpret this plot, it is important to consider an external wave

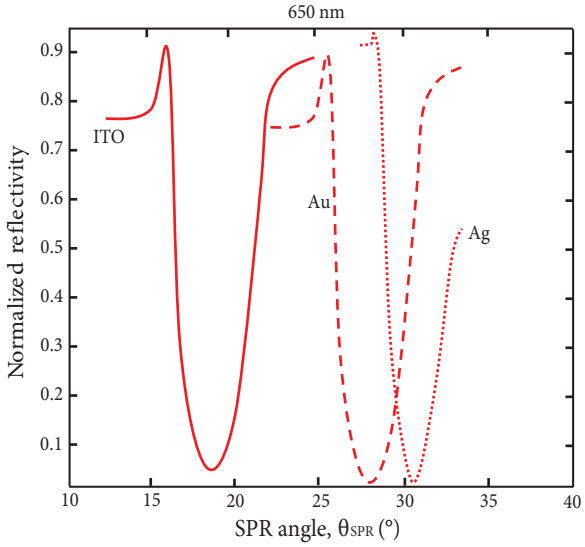

Figure 5. At 650-nm illumination wavelength, measured angular reflectivity curves at Ag (dashed curves), Au (dotted curve), and ITO (solid curve).

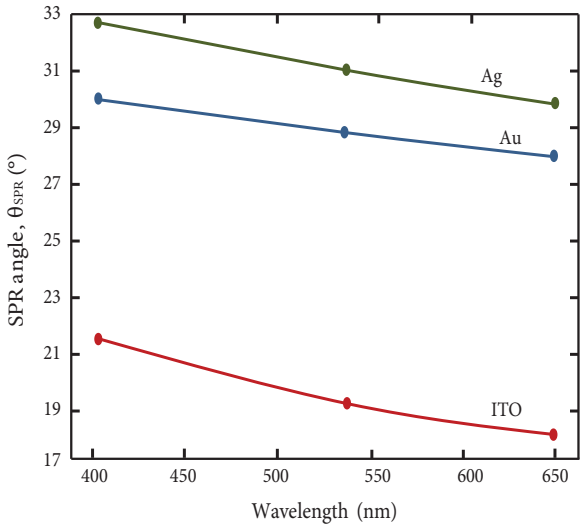

Figure 6. Plots of the measured SPR angle (θ_{SPR}) vs. wavelength (λ) of the incident light for the three prism–metal interfaces (Bp-Ag, Bp-Au, Bp-ITO).

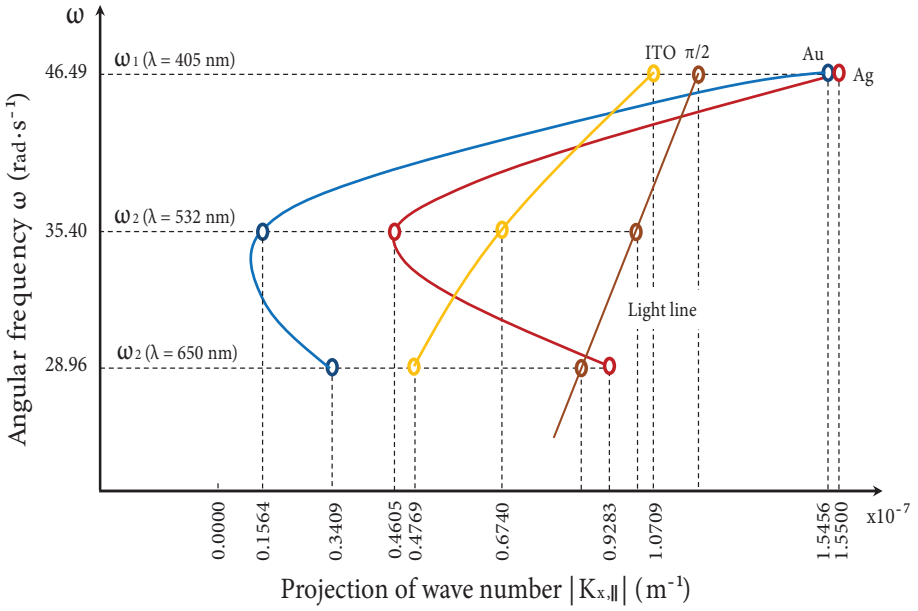

Figure 7. Dispersion relation of the surface plasmon waves at the Bp-Ag, Bp-Au, and Bp-ITO interfaces.

propagating in medium 3 (Figure 1 with a wave vector $k_{x,||}$) impinging on the metallic surface with an incident angle θ. The component of the wave vector parallel to the interface $k_{x,||} = k_x$ can be obtained by the dispersion relation $\omega = (k_x c)/(sin\theta)$, which, in the case of $\theta = \pi/2$, is represented by the light line in Figure 7. As observed in this figure, for the studied incident wavelengths, Bp-ITO is the only prism-metal interface in which surface plasmon dispersion occurs at θ_{SPR} smaller than $\pi/2$. This means that for the Bp-ITO interface the absolute value of the wavenumber projection $|k_{x,||}|$ occurs on the left side of the light line of $\pi/2$. However, for the

interface of Bp-ITO and Bp-Au, the wavenumber projection $|k_{x,||}|$ occurs at a wavelength of 405 nm and 650 nm, and 405 nm at the right side of the light line of $\pi/2$, respectively. Therefore, the plots show that for the Bp-ITO interface, light excitation with θ_{SPR} angles smaller than $\pi/2$ always yields k_x values to couple with the SPW.

5. Conclusions

This paper deals with the study of using transparent ITO film as an alternative metal in a prism-metal interface for SPR generation. The theoretical calculations and experimental measurements of the SPR angle given in an interface of Bp-ITO, Bp-Ag, and Bp-Au were compared. For wavelengths of 405, 532, and 650 nm, the curves obtained from experimental data fit well with the theoretical prediction obtained from calculations. Specifically, the SPR angle in the Bp-ITO interface shows less wavelength sensitivity than Bp-Ag and Bp-Au interfaces. For the case of 405-nm excitation wavelength, the SPR effect is achieved at quite different θ_{SPR} angles for each of the three prism-metal interfaces. This behavior can be attributed to the practical low sensitivity of the Bp-metal interface to optical excitation wavelengths approaching the ultraviolet spectrum. As the optical excitation wavelengths increase, the dispersion of θ_{SPR} angles decrease, demonstrating the high sensitivity of the Bp-metal interface to optical excitation wavelengths approaching the infrared spectrum.

The refraction index of metals strongly influences the SPR generation. As the wavelength of incident light increases, θ_{SPR} decreases. This decrease in θ_{SPR} behavior is similar to the behavior of the real part of the refractive index, which also decreases. Additionally, the dispersion width of the minimum reflectivity increases as the wavelength increases and decreases as the index of refraction increases. Qualitative behaviors of the dispersion relations of the surface plasmon wave at the three studied interfaces demonstrate that light excitation with θ_{SPR} angles smaller than $\pi/2$ always yields k_x values to couple with the SPW. Hence, ITO, which is an economical and very popular compound material, can be used as an alternative to Au and Ag in prism-metal interfaces to generate SPR effects.

Acknowledgment

The authors are grateful to the National Council for Science and Technology of Mexico (CONACYT) for supporting a scholarship for doctoral studies for Adolfo A. Ruiz-Ramirez.

References

[1] Rizal C, Pisana S, Hrvoic I. Improved magneto-optic surface plasmon resonance biosensors. Photonics 2018; 5 (15): 1-16. doi: 10.3390/photonics5030015

[2] Ajiki Y, Kan T, Matsumoto K, Shimoyama I. Electrically detectable surface plasmon resonance sensor by combining a gold grating and a silicon photodiode. Applied Physics Express 2018; 11: 022001. doi: 10.7567/APEX.11.022001

[3] Pockrand I, Swalen JD, Gordon JD 2nd, Philpott MR. Surface plasmon spectroscopy of organic monolayer assemblies. Surface Science 1978; 74: 273-244. doi: 10.1016/0039-6028(78)90283-2

[4] Gordon JD 2nd, Erns S. Surface plasmons as a probe of the electrochemical interface. Surface Science 1980; 101: 499-506. doi: 10.1016/0039-6028(80)90644-5

[5] Liedberg B, Nilander C, Lundstrom I. Biosensing with surface plasmon resonance—how it all started. Biosensors and Bioelectronics 1995; 10: i-ix. doi: 10.1016/0956-5663(95)96965-2

[6] Armelles G, Cebollada A, Garcia-Martin A, González MU. Magnetoplasmonics: combining magnetic and plasmonic functionalities. Advanced Optical Materials 2013; 1: 2–21. doi: 10.1002/adom.201200011

[7] Wolfbeis OS. Fiber-optic chemical sensors and biosensors. Analytical Chemistry 2016; 78 (12): 3859–3874. doi: 10.1021/ac060490z

[8] Brecht A, Gauglitz G. Optical probes and transducers. Biosensors and Bioelectronics 1995; 10: 923–936. doi: 10.1016/0956-5663(95)99230-1

[9] Gauglitz G. Opto-chemical and opto-immuno sensors. Sensors Update 1996; 1 (1): 1–48. doi: 10.1002/1616-8984(199607)1

[10] Peterson AW, Halter M, Plant LA, Elliot J. Surface plasmon resonance microscopy: achieving a quantitative optical response. Review of Scientific Instruments 2016; 87 (9): 093703. doi: 10.1063/1.4962034

[11] Tang Y, Zeng X, Liang J. Surface plasmon resonance: an introduction to a surface spectroscopy technique. Journal of Chemical Education 2010; 87 (7): 742–746. doi: 10.1021/ ed100186y

[12] Homola J, Yee SS, Gauglitz G. Surface plasmon resonance sensors: review. Sensors and Actuators B: Chemical 1999; 54: 3–15. doi: 10.1016/S0925-4005(98)00321-9

[13] Raether H. Surface Plasmons on Smooth and Rough Surfaces and on Gratings. Berlin, Germany: Springer-Verlag, 1988. doi: 10.1007/BFb0048317

[14] Ordal MA, Long LL, Bell RJ, Bell SE, Berll RR et al. Optical properties of metals Al, Co, Cu, Au, Fe, Pb, Ni, Pd, Pt, Ag, Ti, and W in the infrared and far infrared. Applied Optics 1983; 22 (7): 1099-1119. doi: 10.1364/ AO.22.001099

[15] Rizal C, Pisana S, Hrvoic I, Fullerton EE. Microstructure and magneto-optical surface plasmon resonance of Co/Au multilayers. Journal of Physics Communications 2018; 2018: 2055010. doi: 10.1088/0143-0807/32/2/028

[16] Ferreiro-Vila E, Bendana XM, Gonzalez-Diaz JB, Garcia-Martin A, Cebollada A et al. Surface plasmon resonance effects in the magneto-optical activity of Ag/Co/Ag trilayers. IEEE Transactions on Magnetics 2008; 44 (11): 3303–3306. doi: 10.1109/TMAG.2008.2002381

[17] Patskovsky S, Kabashin AV, Meunier M, Luong JHT. Properties and sensing characteristics of surface plasmon resonance in infrared light. Journal of the Optical Society of America A 2003; 20 (8): 1644-1650. doi: 10.1364/JOSAA.20.001644

[18] Hendry E, Carpy T, Johnston J, Popland M, Mikhaylovskiy RV et al. Ultrasensitive detection and characterization of biomolecules using superchiral fields. Nature Nanotechnology 2010; 5 (11): 783-787. doi: 10.1038/nnano. 2010.209

[19] Sipova H, Piliarik M, Vala M, Chadt K, Adam P et al. Portable surface plasmon resonance biosensor for detection of nucleic acids. Procedia Engineering 2011; 25: 148-151. doi: 10.1016/j.proeng.2011.12.037

[20] Pluchery O, Vayron R, Van KM. Laboratory experiments for exploring the surface plasmon resonance. European Journal of Physics 2011; 32 (2): 585-599. doi: 10.1088/0143-0807/32/2/028

[21] Lewis BG, Paine DC. Applications and processing of transparent conducting oxide. MRS Bulletin 2000; 25 (8): 22-27. doi: 10.1557/mrs2000.147

[22] Hossain-Kham MZ, Harkin-Jones E. Effect of ITO surface properties on SAM modification: a review toward biosensors applications. Cogent Engineering 2016; 3 (1): 1170097. doi: 10.1080/23311916.2016. 1170097

[23] Aydin EB, Sezginturk MK, Indium tin oxide (ITO): a promising material in biosensing technology. Trends in Analytical Chemistry 2017; 97: 309-315. doi: 10.1016/j.trac.2017.09.021

[24] Fan X, White IM, Shopova SI, Zhu H, Suter JD et al. Sensitive optical biosensors for unlabeled targets: a review. Analytica Chimica Acta 2008; 620 (1-2): 8-26. doi: /10.1016/j.aca.2008.05.02210

[25] Simon HJ, Mitchell DE, Watson JG. Surface plasmons in silver films – a novel undergraduate experiment. American Journal of Physics 1975; 43 (7): 630-636. doi: 10.1119/1.9764

[26] Caloz C, Itoh T. Electromagnetic Metamaterials: Transmission Line Theory and Microwave Applications. Hoboken, NJ, USA: John Wiley and Sons, 2006. doi: 10.1002/cphc.200600693

[27] Babar S, Weaver JH. Optical constants of Cu, Ag, and Au revisited. Applied Optics 2015; 54 (3): 477-481. doi: 10.1364/AO.54.000477

[28] Werner JG, Knut DP. Refractive Index Profiling Technique. US patent US20100245805A1, 2009.

[29] Whitman PK, Hahn DE, Soules TE, Norton MA, Dixit SN et al. Performance of thin borosilicate glass sheets at 351 nm. In: Boulder Damage Symposium XXXVI; Boulder, CO, USA; 2004.

[30] Fahland M, Vogt T, Schoenberger W, Schiller N. Optical properties of metal based transparent electrodes on polymer films. Thin Solid Films 2008; 516 (17): 5777-5780. doi: 10.1016/j.tsf.2007.10.03222